DEPARTMENT OF INFORMATICS

TECHNISCHE UNIVERSITÄT MÜNCHEN

Bachelor's Thesis in Informatics: Games Engineering

GPU-Accelerated Pressure Solver for Deep Learning

Martin Vincent Wepner

DEPARTMENT OF INFORMATICS

TECHNISCHE UNIVERSITÄT MÜNCHEN

Bachelor's Thesis in Informatics: Games Engineering

GPU-Accelerated Pressure Solver for Deep Learning

GPU-Beschleunigter Druck Löser für Deep Learning

Author:	Martin Vincent Wepner
Supervisor:	Prof. Dr. Nils Thürey
Advisor:	M. Sc. Philipp Holl
Submission Date:	15. March 2019

I confirm that this bachelor's thesis in informatics: games engineering is my own work and I have documented all sources and material used.

Munich, 15. March 2019 Martin Vincent Wepner

Acknowledgments

todo

Abstract

The numerical approximation of Navier-Stokes equations has been a topic of research for a long time. Solving the pressure equation to obtain incompressibility is very compute intensive. Newer approaches optimize this step by training neural networks based on fluid simulations. Φ_{Flow} is a toolkit that is based on the Machine Learning Platform TensorFlow and can simulate fluids fully differentiable. It uses the calculated data during the simulation to adjust the weights of NNs. Its pressure solver is implemented in TensorFlow and thus capable of running on CPUs and GPUs. However, TensorFlow's Dataflow Graph is unnecessarily complex, which slows down the simulation and thus the training of neural networks.

This thesis addresses this performance problem by presenting a TensorFlow Custom Op that solves the pressure efficiently on the GPU. The tailored CSR format was presented, which efficiently stores the Laplace matrix of the pressure to minimize memory access.

My solution outperforms Φ_{Flow}s native TensorFlow implementation by a factor of up to two orders of magnitudes compared to the CPU version and is up to 70 times faster than the GPU version on my test environment.

Das numerische Approximieren der Navier-Stokes Gleichungen ist schon lange ein Thema der Forschung. Das Lösen der Druck Gleichung um Inkompressibilität zu erhalten ist sehr rechenintensiv. Neuere Ansätze optimieren diesen Schritt, indem sie Neuronale Netze auf Basis von Fluid-Simulationen trainieren. Φ_{Flow} ist ein Toolkit, dass auf der Machine Learning Platform TensorFlow aufbaut und Fluide voll differenzierbar simulieren kann. Es kann während der Simulation die berechneten Daten nutzen, um die Gewichte des NNs anzupassen. Der Druck Löser ist in TensorFlow implementiert und damit fähig, auf CPUs und GPUs zu laufen. TensorFlows Dataflow Graph ist aber unnötig komplex, was die Simulation verlangsamt und damit auch das Training der Neuronalen Netze.

Diese Arbeit behandelt dieses Performance Problem, indem sie eine TensorFlow Custom Op präsentiert, die den Druck effizient auf der GPU löst. Hierzu wurde das Zugeschnittene CSR Format vorgestellt, das die Laplace Matrix des Drucks effizient speichert, um die Speicherzugriffe zu minimieren.

Meine Lösung ist bis zu zwei Größenordnungen schneller als die native TensorFlow-Implementierung von Φ_{Flow} im Vergleich zur CPU-Version und bis zu 70 mal schneller als die GPU-Version in meiner Testumgebung.

Contents

1 Introduction

The simulation of fluids is part of our daily life, even if many do not have this in mind. It facilitates the planning phase of vehicles, airplanes and boats by allowing the aerodynamic properties to be determined even before the first prototype has been built [Tsu+09]. A weather forecast as precise as we know it today would not be possible if we could not simulate the air flows of the earth [Kim02]. And the simulation of fluids also plays a role in medicine, for example to better understand blood flow in the human heart [Pes77]. Many designers and artists are working to deliver the greatest possible immersion to the viewer in games and films [Gil09]. Compared to the design for instance of 3D objects, it is very complex and time-consuming to create realistic looking artificial waves with all the splashes and foam [Gil09].

Existing solutions are often very computationally intensive and lead to compromises between speed and accuracy, resolution or size and thus to the believability of the simulation. Especially in games you only have a few milliseconds until the result has to be delivered. Only the immense parallel computing power of graphics cards made it possible to compute dense fluids in real time.

Deep Learning has become state-of-the-art in many areas such as object recognition in recent years [LBH15]. Deep neural networks also appear to be capable of realistically mimicking physical phenomena with the advantage of doing so in a fraction of the time required by conventional solutions [Tom+17] [Thu+18].

1.1 Φ_{Flow}

Φ_{Flow} is a toolkit written in Python and currently under development at the TUM Chair of Computer Graphics and Visualization for solving and visualizing n-dimensional fluid simulations. It focuses on keeping every simulation step differentiable which makes it suitable for backpropagation. Backpropagation is required to calculate the gradient of the loss function of Neural Networks to adjust the weights of the network. Being developed on top of TensorFlow, it is not only capable of running on CPUs, but also completely on GPUs. TensorFlow simplifies the implementation of Machine Learning algorithms including the use of Neural Networks for predictions and classification. This makes Φ_{Flow} a powerful tool to train Neural Networks on fluid simulations and also visualize them by its interactive GUI running in the browser.

1.2 Description of the problem

This work proposes an implementation to solve the pressure equation - the most computationally intensive part of Eulerian fluid simulations. Being as efficient as possible is crucial for fast simulations and thus most importantly for the training of neural networks. Φ_{Flow} already comes with its own pressure solver running directly in TensorFlow. However, TensorFlows dataflow graph is unnecessarily complex which brings overhead to the computation.

TensorFlow offers the possibility to write custom operations ("Custom ops") in C++ to tackle this issue: Writing efficient code to solve a specific problem within the dataflow graph. Furthermore, the CUDA API by Nvidia makes it possible to write low-level CUDA code that runs natively on GPUs. Combining Custom Ops and CUDA kernels lead to a solution that is both efficient and transparent and also compliant to TensorFlow's Tensors which is required within Φ_{Flow}. It can then be compared to the built-in solution of Φ_{Flow}.

1.3 Outline

Chapter 2 discusses past research in this area.
Chapter 3 repeats the theoretical and mathematical background necessary for this work.
In Chapter 4 I present how I improved the Pressure Solve on GPUs.
In chapter 5 I show the results and compare them with those from Φ_{Flow}.
Chapter 6 summarizes and gives suggestions for further work.

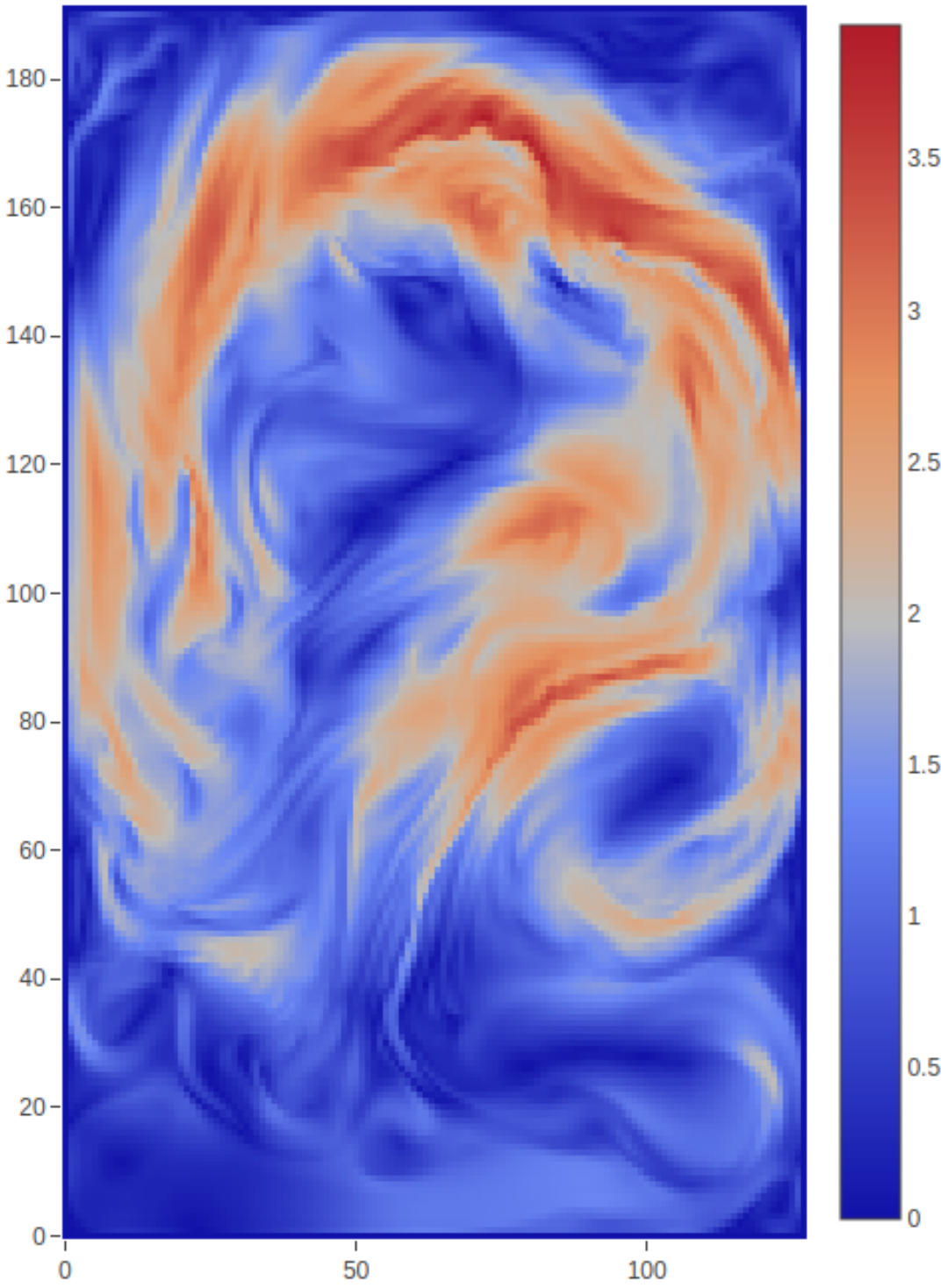

Figure 1.1: Grid-based fluid simulation in Φ_{flow}

2 Related Work

Computational Fluid Dynamics (CFD) has been a research topic long before the first computers appeared. Based on Newton's Second Law, Leonard Euler developed a mathematical model to describe the flow of frictionless inviscid fluids by a set of differential equations in 1757 [Eul57]. Claude Navier and George Stokes extended the Euler Equations by a Viscosity term and formulated the Navier-Stokes-Equations [Nav27] [Sto80]:

$$\frac{\partial \vec{u}}{\partial t} + \vec{u} \cdot \nabla \vec{u} + \frac{1}{\rho} \nabla p = \vec{F} + \nu \nabla \cdot \nabla \vec{u}$$

$$\nabla \cdot u = 0$$

In computer graphics two distinctive approaches have established to numerically approximate the Navier-Stokes-Equations:

Lagragian methods use particles to represent a fluid. The Smoothed Particle Hydrodynamics (SPH) method was presented by Lucy in 1977 to simulate astrophysical problems [Luc77]. In 1992 Monaghan applied the SPH method to fluid dynamics by approximating continuous velocity flow-fields of the Navier-Stokes-Equations using particles with discrete positions and velocities [Mon92]. SPH particles are advected by exerting pressure, viscosity and/or surface tension forces on each other using smoothing kernels [MCG03]. However, it does not fulfill the incompressibility constraint, which can cause undesired visual artifacts. Becker and Teschner presented the weakly compressible SPH system (WCSPH) to maintain incompressibility at the cost of limiting the time-step to impractical sizes [BT07]. Macklin and Mueller introduced Position Based Fluids (PBF), a method which first advects particles and then corrects its positions to satisfy the incompressibility conditions iteratively [MM13]. Several improvements had been done since then and it is still an active topic in research [Mor+].

The alternative to particle-based approaches is the Eulerian viewpoint that splits continuous quantities on a discrete regular grid. First described by Harlow and Welch in 1965 [HW65], they presented the Marker-and-Cell (MAC) grid to prevent biased or null-spaced central differences when advecting velocities. Incompressibility in grid-based approaches is enforced by solving the pressure Poisson equation with a divergence-free velocity field. [TODO: Smth. about CG]

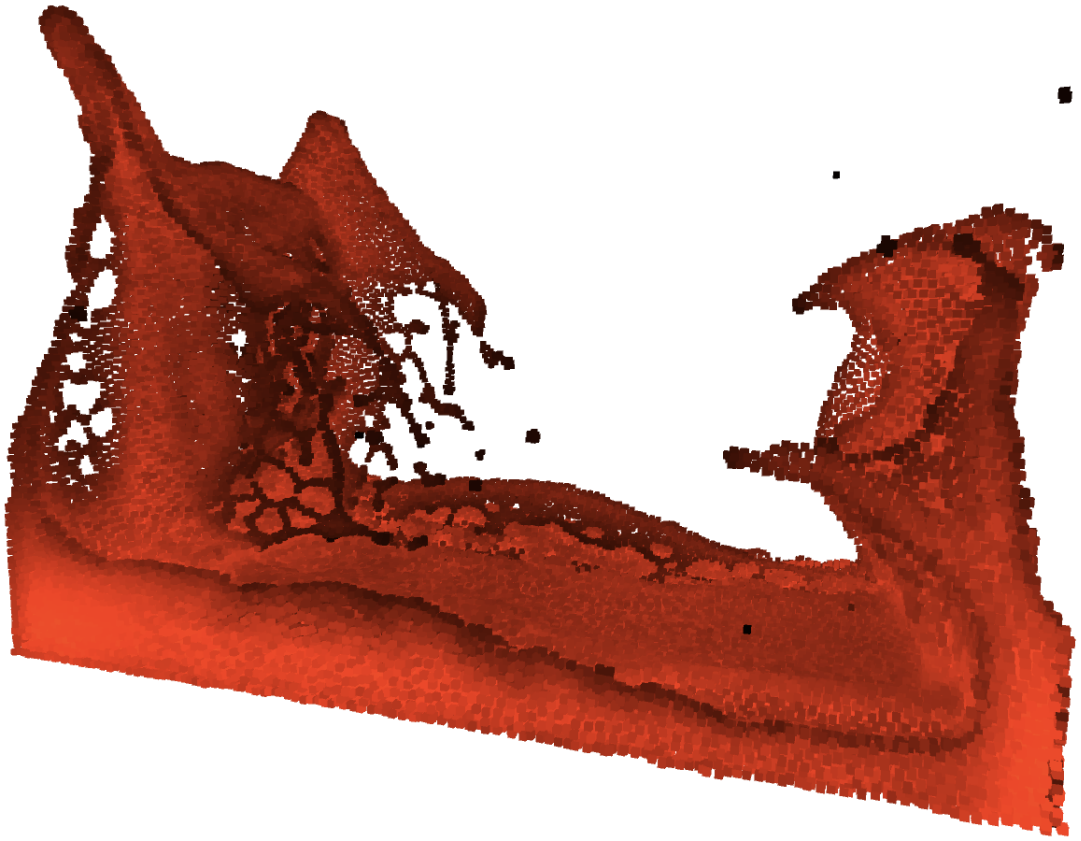

Figure 2.1: Particle-based fluid simulation in Unity3D [Tec19] [Wep17]

Compared to particle-based approaches the grid-based approach achieve higher accuracy. Particle-based methods only needs computation where particles are located; grid-based methods always consider the whole grid.

In the recent years Deep Learning emerged in many fields of research, because GPUs far surpassed the computational capabilities needed to train Neural Networks of multicore CPUs [RMN09]. Deep Neural Networks learn patterns in large data sets by using the backpropagation algorithm and dramatically improved the state-of-the-art in speech recognition, visual object recognition, object detection and many other domains [LBH15]. Furthermore several recent papers have targeted the use of NNs to mimic physical phenomena like rigid-body simulations [Cha+16] and also fluid dynamics [Tom+17] [CT17] [SF18]. Those approaches benefit from the fact, that the evaluation and thus simulation of those NNs are much faster than the conventional mathematical approaches.

3 Numerical approaches for simulating fluids

Incompressible fluids are described by Navier Stokes equations [Nav27] [Sto80]:

$$\frac{\partial \vec{u}}{\partial t} + \vec{u} \cdot \nabla \vec{u} + \frac{1}{\rho} \nabla p = \vec{F} + \nu \nabla \cdot \nabla \vec{u} \tag{3.1}$$

$$\nabla \cdot u = 0 \tag{3.2}$$

Here, $\vec{u}$ denotes the velocity vector of the fluid.
ρ stands for the density of the fluid. E.g. $\rho_{Water} \approx 1000 kg/m^3$.
p, on the other hand, holds the pressure, which is the force per unit the fluid exerts on its surroundings.
$\vec{F}$ denotes external forces such as gravity and buoyancy.
ν is called kinematic viscosity. The higher the viscosity of a fluid is the higher its inherent inertia. For example, honey has a higher viscosity than water.

Equation 3.1 - the "momentum equation" - very briefly describes how the fluid accelerates due to the forces acting on it. eq. 3.2 is called "incompressibility condition" and means that the "volume?!" of the fluid doesn't change.

If real fluids were incompressible, we couldn't hear anything underwater [Uri67], so why do we assume them to be incompressible? Liquids are practically incompressible - it requires a lot of force to do so, and it is also only possible up to a small degree of compression [Kel75]. Gases like air are easier to compress, but only with the help of pumps [Bur78] or extreme situations like blast waves caused by for example explosions [Tay50a] [Tay50b]. Those kind of scenarios are called "compressible flow" and are expensive to simulate [PL92]. Additionally, they are only visible on a macroscopic level and hence irrelevant for the animation of fluids [Bri15].

Viscosity needs to be considered only in those cases where animating viscous fluids like honey is desired [Bri15]. For most cases, however, it plays a minor role and can be dropped. Those ideal fluids without viscosity are called "inviscid". The Navier Stokes

equations can then be simplified to the following, the so-called "Euler Equations":

$$\frac{\partial \vec{u}}{\partial t} + \frac{1}{\rho}\nabla p = \vec{F} \tag{3.3}$$

$$\nabla \cdot u = 0 \tag{3.4}$$

3.1 The role of the pressure solve in incompressible Navier Stokes equations

In this section, we briefly derive a numerical approximation for the pressure equation of the Navier Stokes equations with the help of a MAC-grid for two-dimensional simulations. Bridson [Bri15] [BM07] already explained this for both 2D and 3D in detail.

3.1.1 Discretization and derivation of the pressure equation

Discretizing eq. 3.3 and 3.4 in time and space gives for a discrete point in time n the following equations:

$$\vec{u}^{n+1} = \vec{u}^{n} - \Delta t \frac{1}{\rho}\nabla p \quad s.t. \quad \nabla \cdot \vec{u}^{n+1} = 0 \tag{3.5}$$

The divergence of a two dimensional vector $\vec{u} = (u, v)$ is defined as

$$\nabla \cdot \vec{u} = \frac{\partial u}{\partial x} + \frac{\partial v}{\partial y} \tag{3.6}$$

So for a fluid grid cell (i, j):

$$(\nabla \cdot \vec{u})_{i,j} = \frac{u^{n+1}_{i+1/2,j} - u^{n+1}_{i-1/2,j}}{\Delta x} + \frac{v^{n+1}_{i,j+1/2} - v^{n+1}_{i,j-1/2}}{\Delta x} + \mathcal{O}(\Delta x^2) \tag{3.7}$$

Using the central difference for $\frac{\partial p}{\partial x}$ and $\frac{\partial p}{\partial y}$ the velocity update is:

$$u^{n+1}_{i+1/2,j} = u^{n}_{i+1/2,j} - \Delta t \frac{1}{\rho}\frac{p_{i+1,j} - p_{i,j}}{\Delta x} \tag{3.8}$$

$$v^{n+1}_{i+1/2,j} = v^{n}_{i,j+1/2} - \Delta t \frac{1}{\rho}\frac{p_{i,j+1/2} - p_{i,j}}{\Delta x} \tag{3.9}$$

Substituting 3.8 and 3.9 into 3.7 finally gives:

$$\frac{1}{\Delta x}\left[\left(u^n_{i+1/2,j} - \Delta t\frac{1}{\rho}\frac{p_{i+1,j}-p_{i,j}}{\Delta x}\right) - \left(u^n_{i-1/2,j} - \Delta t\frac{1}{\rho}\frac{p_{i-1,j}-p_{i,j}}{\Delta x}\right)\right.$$
$$\left. + \left(v^n_{i,j+1/2} - \Delta t\frac{1}{\rho}\frac{p_{i,j+1}-p_{i,j}}{\Delta x}\right) - \left(v^n_{i,j-1/2} - \Delta t\frac{1}{\rho}\frac{p_{i,j-1}-p_{i,j}}{\Delta x}\right)\right] = 0$$

$$-4p_{i,j} + p_{i+1,j} + p_{i,j+1} + p_{i-1,j} + p_{i,j-1} = \frac{\rho\Delta x}{\Delta t}\left(u^n_{i+1/2,j} - u^n_{i-1/2,j} + v^n_{i,j+1/2} - v^n_{i,j-1/2}\right) \tag{3.10}$$

Now we have a system of linear equations in the form of the Poisson problem:

$$\mathbf{A}\vec{p} = \frac{\rho\Delta x^2}{\Delta t}\nabla\cdot\vec{u}^n \tag{3.11}$$

The Laplace Matrix **A** is a symmetric and positive semi-definite matrix so eq. 3.11 can therefore be solve by the Conjugate Gradient method. Each row in **A** represents one cell (i, j) on the MAC-grid.

3.1.2 Boundary Conditions

Solids

If an inviscid fluid is in contact with a wall, it cannot move into or out of the boundary. To achieve this the velocity components of the solid normal needs to match the speed of the fluid at this position:

$$\vec{u}\cdot\hat{n} = \vec{u}_{solid}\cdot\hat{n} \tag{3.12}$$

Concerning the pressure update, assume grid cell (i, j) to be fluid and its neighbor $(i+1, j)$ to be solid. Then $u^{n+1}_{i+1/2,j} = u_{solid}$ and 3.8 can be rearranged to

$$p_{i+1,j} = p_{i,j} + \frac{\rho\Delta x}{\Delta t}(u_{i+1/2,j} - u_{solid}) \tag{3.13}$$

This is called Neumann boundary condition because the derivative of the solution is specified along the boundary.

Open/Air

Compared to water, air is about 780 times lighter. When simulating liquids, the pressure p of air regions may be set to zero since it has only minimal impact and therefore no significant visual effect. Since we directly specify the value of the pressure at those air cells it is called a Dirichlet boundary condition.

Extended MAC-grid

From equation 3.10 we know that for one pressure update of one cell we need to consider all its neighbors. What about those grid cells lying on the edge of the grid? Technically those cells have fewer neighbors than the others. To solve this issue, we extend the grid that holds the information about the state (fluid, solid, air) on every dimension. So for a (n x m) sized simulation, we need an (n+2 x m+2) grid that holds the information. We differ between open boundaries where those extended cells are just air cells and closed boundaries where solid cells surround the grid.

3.2 The Laplace Matrix

To implement a method that extracts the Laplace Matrix **A**, we need to take a look on the boundary conditions first. Assume a grid cell (i, j) of which one neighbor $(i-1, j)$ is an air cell ($p_{i-1,j} = 0$) and another $(i+1, j)$ is a solid cell ($p_{i+1,j} = p_{i,j} + \frac{\rho \Delta x}{\Delta t}(u_{i+1/2,j} - u_{solid})$). The remaining neighbors are fluid cells. Knowing that, we can rearrange 3.10 to the following:

$$\begin{aligned} &-4p_{i,j} + \left[p_{i,j} + \frac{\rho \Delta x}{\Delta t}(u_{i+1/2,j} - u_{solid})\right] + p_{i,j+1} + 0 + p_{i,j-1} \\ &= \frac{\rho \Delta x^2}{\Delta t}\left(\frac{u^n_{i+1/2,j} - u^n_{i-1/2,j}}{\Delta x} + \frac{v^n_{i,j+1/2} - v^n_{i,j-1/2}}{\Delta x}\right) \end{aligned} \tag{3.14}$$

which results in

$$-3p_{i,j} + p_{i,j+1} + p_{i,j-1} = \frac{\rho \Delta x^2}{\Delta t}\left(\frac{u^n_{solid} - u^n_{i-1/2,j}}{\Delta x} + \frac{v^n_{i,j+1/2} - v^n_{i,j-1/2}}{\Delta x}\right) \tag{3.15}$$

We can make some very important observations from 3.10, 3.14 and 3.15 for building the Laplace Matrix in code:

- Every row in **A** represents one cell (i, j) and every column all cells on the MAC-grid. Non-neighbor entries of **A** are 0.
- Note that the coefficient of $p_{i,j}$ in 3.10 matches the negative number of neighbors of a cell (i, j). Let's call this coefficient $k_{diagonal} = -dim(grid) * 2$, since it is always on the diagonal of **A**'s entries.
- Every neighbor of cell (i, j) is 1 in the corresponding row of **A**.
- For every neighbor of cell (i, j) that is a solid cell increment $k_{diagonal}$ by 1 and set the corresponding column to 0.
- For every neighbor of cell (i, j) that is an open cell set the corresponding column to 0.
- In liquid simulations: For every neighbor of cell (i, j) that is an air cell set the corresponding column to 0.

With that in mind, we can derive an algorithm which builds **A**. Note that most of **A** is zero so it is a sparse matrix. Also, because of the symmetry of neighboring cells, **A** is symmetric.

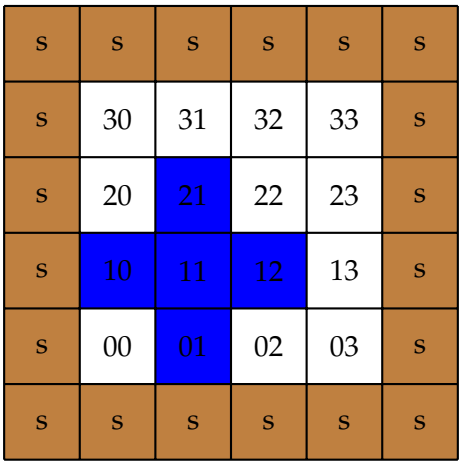

Figure 3.1: Example grid with fluid (blue), air (white) and solid (brown) cells and a closed boundary.

$$
\begin{array}{c|cccccccccccccccc}
 & 00 & 01 & 02 & 03 & 10 & 11 & 12 & 13 & 20 & 21 & 22 & 23 & 30 & 31 & 32 & 33 \\
00 & -2 & 1 & & & 1 & & & & & & & & & & & \\
01 & 0 & -3 & 0 & & & 1 & & & & & & & & & & \\
02 & & 1 & -3 & 0 & & & 1 & & & & & & & & & \\
03 & & & 0 & -2 & & & & 0 & & & & & & & & \\
10 & 0 & & & & -3 & 1 & & & 0 & & & & & & & \\
11 & & 1 & & & 1 & -4 & 1 & & & 1 & & & & & & \\
12 & & & 0 & & & 1 & -4 & 0 & & & 0 & & & & & \\
13 & & & & 0 & & & 1 & -3 & & & & 0 & & & & \\
20 & & & & & 0 & & & & -3 & 1 & & & 0 & & & \\
21 & & & & & & 1 & & & 0 & -4 & 0 & & & 0 & & \\
22 & & & & & & & 1 & & & 1 & -4 & 0 & & & 0 & \\
23 & & & & & & & & 0 & & & 0 & -3 & & & & 0 \\
30 & & & & & & & & & 0 & & & & -2 & 0 & & \\
31 & & & & & & & & & & 1 & & & 0 & -3 & 0 & \\
32 & & & & & & & & & & & 0 & & & 0 & -3 & 0 \\
33 & & & & & & & & & & & & 0 & & & 0 & -2
\end{array}
\cdot
\begin{pmatrix} p_{0,0} \\ p_{0,1} \\ p_{0,2} \\ p_{0,3} \\ p_{1,0} \\ p_{1,1} \\ p_{1,2} \\ p_{1,3} \\ p_{2,0} \\ p_{2,1} \\ p_{2,2} \\ p_{2,3} \\ p_{3,0} \\ p_{3,1} \\ p_{3,2} \\ p_{3,3} \end{pmatrix}
$$

Figure 3.2: Laplace Matrix **A** derived from Fig. 3.1 with corresponding pressure vector. Diagonal are marked as red, neighbors as blue and non neighbors are left out.

4 CUDA Pressure Solver

In this chapter, we find an efficient numerical approach to solve the system of linear equations $\mathbf{A}\vec{p} = \frac{\rho\Delta x^2}{\Delta t}\nabla \cdot \vec{u}^n$ (3.11) using TensorFlows Custom Ops and Nvidia CUDA Kernels. First, we discuss how $\mathbf{A}$ is built and stored in memory and then how the Conjugate Gradient method can be used to solve it.

We will use some recurring variables which I clarify here:

- *dimensions* is an array which holds the size of each dimension of the grid.
- *dimSize* holds the number of dimensions.
- *dimProduct* is the product $\prod_{i=0}^{dimSize} dimensions[i]$ of all dimensions.
- *mask* holds the information of fluid, open and solid cells including the boundary cells.
- *maskDimensions* is an array that holds the dimensions of the mask.

4.1 GPU Laplace Matrix generation

The goal of this section is to find a parallelizable algorithm that creates the Laplace Matrix A, so that a GPU can compute exactly one cell (i, j) or one row of $\mathbf{A}$ per thread.

GPU memory is very limited. For a simulation of the size 64 x 64 x 64 the dimension of the Laplace Matrix is 262.144 x 262.144. This would require 256 gigabyte of GPU-memory if we tried to cache the matrix with 32 bit numbers. At the time of this writing this is only possible with special GPUs that have additional GPU-SSD memory.

Take a look back on the example Laplace Matrix in Fig. 3.2. Notice, that most of it is zero. In fact, there are only at most as many non-zero entries as the number of neighbors of a cell plus one for the cell itself:

$$maxNonZerosPerRow = dimSize * 2 + 1 \tag{4.1}$$

For 2D this means at most five and for 3D at most seven entries per row.

$$\begin{pmatrix} 4 & 0 & 0 & 0 & 0 & 0 \\ 1 & 4 & 0 & 0 & 0 & 0 \\ 0 & 0 & 4 & 0 & 0 & 0 \\ 3 & 0 & 0 & 4 & 0 & 0 \end{pmatrix} \quad \begin{aligned} \textit{data} &= [4,1,4,4,3,4] \\ \textit{columnptr} &= [0,0,1,2,0,3] \\ \textit{rowcnt} &= [0,1,3,4,6] \end{aligned}$$

Figure 4.1: Example Matrix in CSR format

The *compressed sparse row* (CSR) [TW67] format tackles this memory problem by only storing information of non-zero entries of a sparse matrix. It consists of three arrays:

data:	values of non-zero entries in row-major order.
columnptr:	the column indices of all non-zero data entries in row-major order.
rowcnt:	The *i*th element points to the index in *data* of the first non-zero entry of the *i*th row.

Because **A** is sparse to a vast extent, the CSR format reduces memory consumption dramatically. However, it requires three memory accesses to get all data of one entry. Compared to pure computation, memory accesses are very costly on GPUs and should be kept as low as possible [Fan+18][Fuj+13]. To improve speed, reducing those memory accesses is crucial.

4.1.1 Tailoring the CSV format for the GPU pressure solve

For every row i we know that all non-zero entries of this row lay in the range $\big[\textit{rowcnt}[\text{i}]\ ;\ \textit{rowcnt}[\text{i+1}]\big[$ in the *data* array.

The maximum number of non-zero entries per row in the Laplace Matrix is $maxNonZerosPerRow$ as defined above. It is only the maximum possible number of non-zeros because neighbor cells of (i,j) might be open or solid cells, thus zero in the (i,j)th row of the Laplace Matrix. For cells at the edge of the grid, we set the corresponding value for neighbor cells that lay outside the grid to zero in the *data* array as well. The CSR format would have removed those zero entries but if we keep them, we have a regular arrangement of *data* ($data_{regular}$)-entries per row. As a trade-of this will require slightly more memory. However we are now able to calculate the index of the row i_{row} of any *data* entry by its index i_{data}:

$$i_{row} = \left\lfloor \frac{i_{data}}{maxNonZerosPerRow} \right\rfloor \tag{4.2}$$

For efficient parallelizing, this step is indispensable. If the GPU executes two cells for example $(i+1,j)$ and (i,j) in two threads at the same time and every *data* entry does not have a predefined place in the array, the threads would mix up their insertions and thus the row-major structure. Since $data_{regular}$ is now regular, each thread knows the exact position in $data_{regular}$ for every entry to comply the row-major order.

$$data = \Big[\underbrace{0, 0, -2, 1, 1}_{i_{row}=0} \ , \ \underbrace{0, 0, -3, 0, 1}_{i_{row}=1} \ , \ \underbrace{0, 0, -3, 0, 1}_{i_{row}=2} \ , \ \underbrace{0, 0, -2, 0, 0}_{i_{row}=3} \ , \ \underbrace{0, 0, -3, 1, 0}_{i_{row}=4} \ , \ \dots \Big]$$

Figure 4.2: Vizualization of $data_{regular}$ array for Fig. 3.2. Diagonal entries are printed in red. Neighbor cells are printed in blue if they are within the grid and brown otherwise.

$$diagonalOffset = [\ -4, -1, 0, 1, 4\ ]$$

Figure 4.3: $diagonalOffset$ array that corresponds to Fig. 3.2.

More in-depth inspection of Fig. 3.2 reveals that neighbor-cell entries always appear by the same distances to the diagonal of each row. Of course, this is due to the fact that the respective neighbors on the linearized grid lie at the same distance from each other for every cell accordingly. This is also applicable to the $data_{regular}$ array: in respect to the diagonal (red) entries the neighbors always appear in the same order (Fig. 4.3). With this knowledge we can extract a method to infer from each $data_{regular}$ entry the respective column index i_{column} via the data index i_{data}.

To do this, we define a new helper array $diagonalOffsets$ which stores the column-index distance to the diagonal of every entry of a row. Here is an algorithm to create the $diagonalOffsets$ array:

Algorithm 1 Creates an array containing the column offset for every neighbor of a row in **A** in respect to the diagonal

```
1:  function GET DIAGONALOFFSETS(maxDataPerRow, dimensions )
2:      offsets = [i_0, i_1, ··· , i_maxDataPerRow]   ▷ Declare array of length maxDataPerRow
3:      factor = 1
4:      const diagonal = ⌊maxNonZerosPerRow / 2⌋
5:
6:      for i = 0, offset = 1; i < diagonal; i++, offset++ do
7:          offsets[diagonal − offset] = −factor
8:          offsets[diagonal + offset] = factor
9:          factor = factor ∗ dimensions[i]
10:     offsets[diagonal] = 0
11:     return offsets
```

Now getting the column index i_{column} by an arbitrary $data_{regular}$ index i_{data} is trivial:

$$\begin{aligned} i_{column} &= \left\lfloor \frac{i_{data}}{maxNonZerosPerRow} \right\rfloor && + columnOffsets\,[i_{data} \mod maxNonZerosPerRow] \\ &= i_{row} && + columnOffsets\,[i_{data} \mod maxNonZerosPerRow] \end{aligned} \tag{4.3}$$

4.2 GPU Pressure Solve

In the previous section we found an algorithm that creates and stores the Laplace Matrix efficiently on GPUs. In this section I present how the system of linear equations $\mathbf{A}\vec{p} = \frac{\rho \Delta x^2}{\Delta t} \nabla \cdot \vec{u}^n$ (3.11) can be solved on GPUs using the Conjugate Gradient method. First, we simplify equation 3.11:

$$\mathbf{A}\vec{p} = \vec{d} \tag{4.4}$$

Now solving this system of linear equations with the cg-method works as follows:

Algorithm 2 Pressure Solve with cg-method

1: **function** SOLVE PRESSURE($\mathbf{A}$, $\vec{d}$, $maxIterations$, $accuracy$, $\vec{p}_0$)
2: $\quad \vec{m} = \vec{r} = \vec{d} - \mathbf{A}\vec{p}_0$ ▷ Init helper variables
3: $\quad \vec{p} = \vec{p}_0$
4: $\quad$ **for** $k = 1$ to $maxIterations$ **do**
5: $\quad\quad \vec{z} = \mathbf{A}\vec{m}$ ▷ calcZ
6: $\quad\quad alpha = \frac{\vec{m} \bullet \vec{r}}{\vec{m} \bullet \vec{z}}$
7: $\quad\quad \vec{p} = \vec{p} + alpha \cdot \vec{m}$
8: $\quad\quad \vec{r} = \vec{r} - alpha \cdot \vec{z}$
9: $\quad\quad$ **if** $max_i(|\vec{r}_i|) < accuracy$ **then** ▷ checkResiduum
10: $\quad\quad\quad$ **return** $\vec{p}$
11: $\quad\quad beta = -\frac{\vec{r} \bullet \vec{z}}{\vec{m} \bullet \vec{z}}$
12: $\quad\quad \vec{m} = \vec{r} + beta \cdot \vec{m}$
13: $\quad$ **return** $\vec{p}$

All mathematical operations except for operation 5 and 9 can be executed by the highly optimized cuBLAS library which is part of CUDAs standard libraries.
Obviously operation 5 is the most demanding because it involves a matrix-vector multiplication. Now we can take advantage of the findings and optimization steps in the previous section.

calcZ

Without further ado, we can derive an algorithm to calculate $\vec{z}$ using **A** in the Tailored CSR format. Every thread computes one entry of the resulting vector. The row $rowID$ of this vector is given by the CUDA thread and block id:

Algorithm 3 Multiplies **A** with a vector

```
1: function CALCZ(rowID, A, m, z, columnOffsets )
2:     if rowID < dimProduct then
3:         rowStartIndex = rowID * maxNonZerosPerRow
4:         tmp = 0
5:         for i = rowStartIndex; i < rowStartIndex + maxNonZerosPerRow; i++ do
6:             tmp = tmp + A[i] · m[rowID + columnOffsets[i − rowStartIndex]]
7:         z[rowID] = tmp
```

checkResiduum

The cg-method approximates the solution of a system of linear equations iteratively. It should terminate if all entries of the residuum vector $\vec{r}$ is smaller than the given *accuracy*. We introduce a new variable $finished$ and set it to true at the beginning of every cg-iteration. The checkResiduum method searches for an entry in $\vec{r}$ to be greater than *accuracy* in parallel. Every match sets $finished$ to false. When all checks have been done we can break the cg-iteration if $finished$ is still true.

5 Results

In this chapter I present how my CUDA solution compares against the TensorFlow implementations of Φ_{Flow}.

All benchmarks were performed in a closed boundary environment with random divergence vectors in the $[-1, 1]$ range. The targeted residual accuracy was 1^{-5}. Before starting the measurement, a warm-up of 5 runs was performed. The data shows the mean and standard deviation of 25 runs. The test system consists of a GeForce GTX 980, a Quad-Core Intel Core i7 3779K @3.5GHz CPU and 8GB of RAM.

Performance Pressure Solve

The following table shows the execution time per solve (t/s) and the average number of cg-iterations (iters) for quadratic grids and compares the Tensorflow solutions with my CUDA implementation:

Dimension	TF CPU		TF GPU		CUDA		Speedup CPU	Speedup GPU
	t/s	iters	t/s	iters	t/s	iters		
64^2	49,65 ms		108,2 ms		25,36 ms		2.0 x	4.2 x
128^2	207,6 ms		396,3 ms		39,49 ms		5.3 x	10.0 x
256^2	1,169 s		1,839 s		77,19 ms		15.1 x	23.8 x
512^2	12,75 s		12,90 s		240,9 ms		52.9 x	53.6 x
1024^2	133.7 s		87,47 s		1,412 s		94.6 x	61.9 x
2048^2	n/a		n/a		9,742 s		n/a	n/a
64^3	3,878 s		2,473 s		42,18 ms		91.9 x	58.6 x
128^3	55.22 s		29,35 s		397,1 ms		139.1 x	73.9 x
256^3	n/a		n/a		5,814 s		n/a	n/a

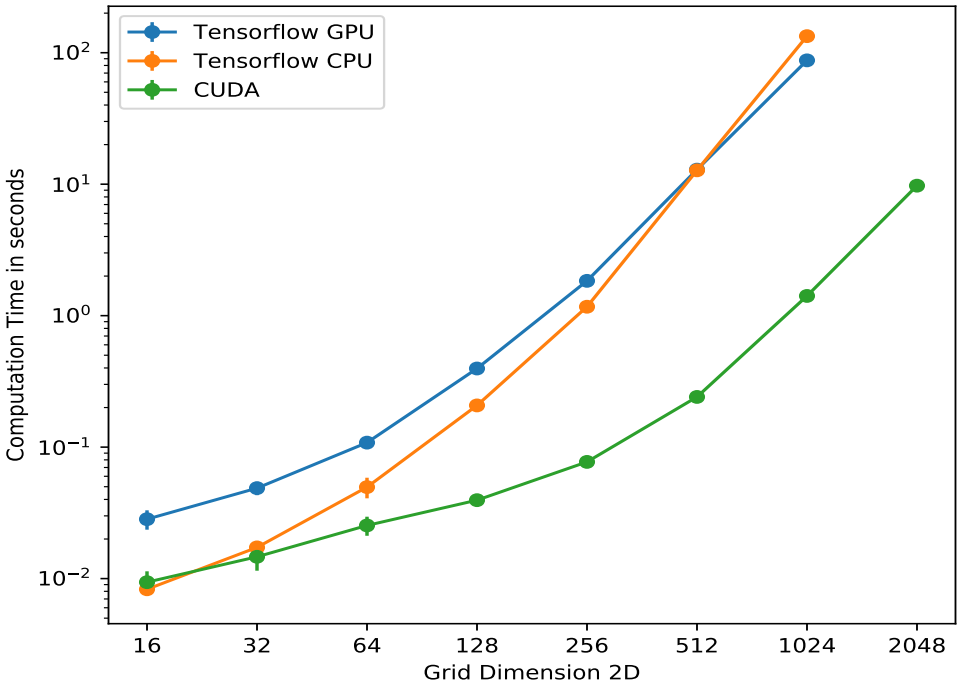

(a) Pressure Solve in 2D

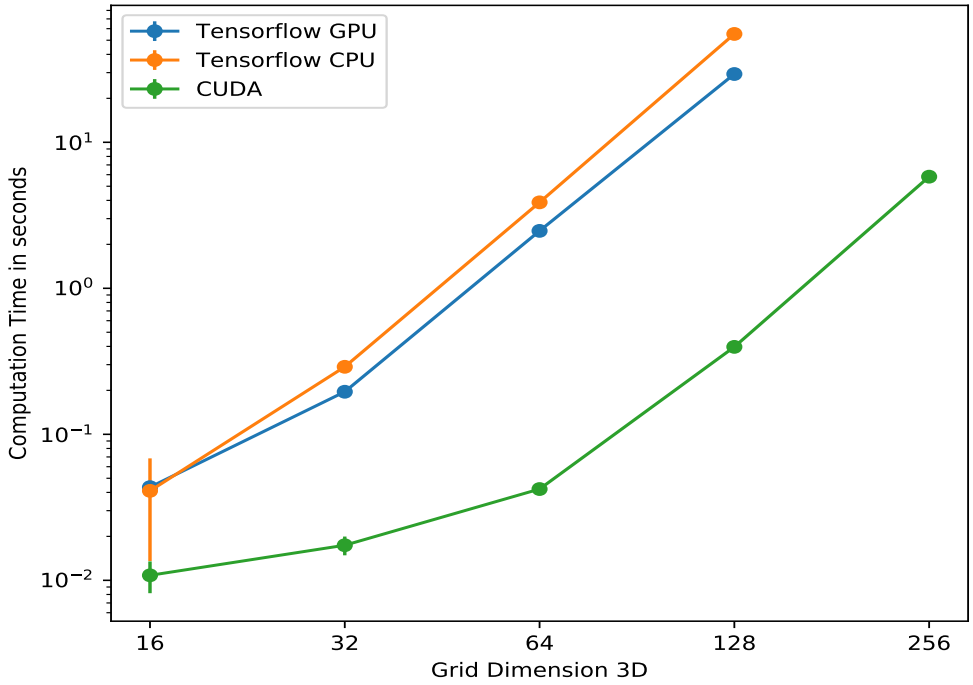

(b) Pressure Solve in 3D

Figure 5.1: Execution time comparison between the three solvers and batch size 1.

6 Conclusion and Future Work

In this thesis I presented an efficient implementation for the pressure solver. I introduced the Tailored CSR format that allows the Laplace Matrix to be created efficiently on the GPU with little memory used. This allows the matrix multiplication in the cg-method to be calculated faster than conventional methods. The highly optimized cuBLAS library can execute all other mathematical operations efficiently on the GPU.

I was able to improve the speed by a factor of up to 139 compared to the CPU version and by a factor of up to 72 compared to the Φ_{flow} TensorFlow implementation.

Because the main focus of this work was the acceleration of the pressure solver, there is still potential to improve the Laplace matrix generation kernel. In addition, there are certainly possibilities to further optimize memory access in the cg algorithm.

Bibliography

[BM07] R. Bridson and M. Müller-Fischer. "Fluid simulation: SIGGRAPH 2007 course notes Video files associated with this course are available from the citation page." In: *ACM SIGGRAPH 2007 courses*. ACM. 2007, pp. 1–81.

[Bri15] R. Bridson. *Fluid simulation for computer graphics*. AK Peters/CRC Press, 2015.

[BT07] M. Becker and M. Teschner. "Weakly compressible SPH for free surface flows." In: *Proceedings of the 2007 ACM SIGGRAPH/Eurographics symposium on Computer animation*. Eurographics Association. 2007, pp. 209–217.

[Bur78] T. I. Burenga. *Portable air compressor*. US Patent 4,077,747. Mar. 1978.

[Cha+16] M. B. Chang, T. Ullman, A. Torralba, and J. B. Tenenbaum. "A compositional object-based approach to learning physical dynamics." In: *arXiv preprint arXiv:1612.00341* (2016).

[CT17] M. Chu and N. Thuerey. "Data-driven synthesis of smoke flows with CNN-based feature descriptors." In: *ACM Transactions on Graphics (TOG)* 36.4 (2017), p. 69.

[Eul57] L. Euler. "Principes généraux du mouvement des fluides." In: *Mémoires de l'Académie des Sciences de Berlin* (1757), pp. 274–315.

[Fan+18] M. Fang, J. Fang, W. Zhang, H. Zhou, J. Liao, and Y. Wang. "Benchmarking the GPU memory at the warp level." In: *Parallel Computing* 71 (2018), pp. 23–41.

[Fuj+13] Y. Fujii, T. Azumi, N. Nishio, S. Kato, and M. Edahiro. "Data transfer matters for GPU computing." In: *2013 International Conference on Parallel and Distributed Systems*. IEEE. 2013, pp. 275–282.

[Gil09] J. Gilland. *Elemental magic: the art of special effects animation*. 2009.

[HW65] F. H. Harlow and J. E. Welch. "Numerical calculation of time-dependent viscous incompressible flow of fluid with free surface." In: *The physics of fluids* 8.12 (1965), pp. 2182–2189.

[Kel75] G. S. Kell. "Density, thermal expansivity, and compressibility of liquid water from 0. deg. to 150. deg.. Correlations and tables for atmospheric pressure and saturation reviewed and expressed on 1968 temperature scale." In: *Journal of Chemical and Engineering Data* 20.1 (1975), pp. 97–105.

[Kim02] R. Kimura. "Numerical weather prediction." In: *Journal of Wind Engineering and Industrial Aerodynamics* 90.12-15 (2002), pp. 1403–1414.

[LBH15] Y. LeCun, Y. Bengio, and G. Hinton. "Deep learning." In: *nature* 521.7553 (2015), p. 436.

[Luc77] L. B. Lucy. "A numerical approach to the testing of the fission hypothesis." In: *The astronomical journal* 82 (1977), pp. 1013–1024.

[MCG03] M. Müller, D. Charypar, and M. Gross. "Particle-based fluid simulation for interactive applications." In: *Proceedings of the 2003 ACM SIGGRAPH/Eurographics symposium on Computer animation*. Eurographics Association. 2003, pp. 154–159.

[MM13] M. Macklin and M. Müller. "Position based fluids." In: *ACM Transactions on Graphics (TOG)* 32.4 (2013), p. 104.

[Mon92] J. J. Monaghan. "Smoothed particle hydrodynamics." In: *Annual review of astronomy and astrophysics* 30.1 (1992), pp. 543–574.

[Mor+] D. Morikawa, M. Asai, Y. Imoto, M. Isshiki, et al. "Improvements in highly viscous fluid simulation using a fully implicit SPH method." In: *Computational Particle Mechanics* (), pp. 1–16.

[Nav27] C. L. Navier. *Mémoire sur les lois de l'équilibre et du mouvement des corps solides élastiques*. 1827.

[Pes77] C. S. Peskin. "Numerical analysis of blood flow in the heart." In: *Journal of computational physics* 25.3 (1977), pp. 220–252.

[PL92] T. J. Poinsot and S. Lelef. "Boundary conditions for direct simulations of compressible viscous flows." In: *Journal of computational physics* 101.1 (1992), pp. 104–129.

[RMN09] R. Raina, A. Madhavan, and A. Y. Ng. "Large-scale deep unsupervised learning using graphics processors." In: *Proceedings of the 26th annual international conference on machine learning*. ACM. 2009, pp. 873–880.

[SF18] C. Schenck and D. Fox. "Spnets: Differentiable fluid dynamics for deep neural networks." In: *arXiv preprint arXiv:1806.06094* (2018).

[Sto80] G. G. Stokes. "On the theories of the internal friction of fluids in motion, and of the equilibrium and motion of elastic solids." In: *Transactions of the Cambridge Philosophical Society* 8 (1880).

[Tay50a] G. I. Taylor. "The formation of a blast wave by a very intense explosion I. Theoretical discussion." In: *Proceedings of the Royal Society of London. Series A. Mathematical and Physical Sciences* 201.1065 (1950), pp. 159–174.

[Tay50b] G. I. Taylor. "The formation of a blast wave by a very intense explosion.-II. The atomic explosion of 1945." In: *Proceedings of the Royal Society of London. Series A. Mathematical and Physical Sciences* 201.1065 (1950), pp. 175–186.

[Tec19] U. Technologies. *Unity3D*. `https://unity3d.com/`. 2019.

[Thu+18] N. Thuerey, K. Weissenow, H. Mehrotra, N. Mainali, L. Prantl, and X. Hu. "Well, how accurate is it? a study of deep learning methods for reynolds-averaged navier-stokes simulations." In: *arXiv preprint arXiv:1810.08217* (2018).

[Tom+17] J. Tompson, K. Schlachter, P. Sprechmann, and K. Perlin. "Accelerating eulerian fluid simulation with convolutional networks." In: *Proceedings of the 34th International Conference on Machine Learning-Volume 70*. JMLR. org. 2017, pp. 3424–3433.

[Tsu+09] M. Tsubokura, T. Kobayashi, T. Nakashima, T. Nouzawa, T. Nakamura, H. Zhang, K. Onishi, and N. Oshima. "Computational visualization of unsteady flow around vehicles using high performance computing." In: *Computers & Fluids* 38.5 (2009), pp. 981–990.

[TW67] W. F. Tinney and J. W. Walker. "Direct solutions of sparse network equations by optimally ordered triangular factorization." In: *Proceedings of the IEEE* 55.11 (1967), pp. 1801–1809.

[Uri67] R. J. Urick. *Principles of underwater sound for engineers*. Tata McGraw-Hill Education, 1967.

[Wep17] M. Wepner. *SPH in Unity3D*. `https://martin-wepner.de/fluid-simulation-with-compute-shader/`. 2017.